DOI: 10.1002/stco.202500021

Adrian Münch, Philipp Weidner, Thomas Ummenhofer

ARTICLE

Experimental investigations of N-joints made of high-strength hollow sections

This article presents experimental investigations of the structural behaviour of welded N-joints made of high-strength hollow sections. A total of 13 large-scale tests were carried out on joints made from five different steel grades (S500MH, S620QH, S700MH, S770QH and S890QH) using both circular (CHS) and square (SHS) hollow sections. All specimens have been produced with full penetration butt welds to avoid weld failure and isolate punching shear failure (PSF) and chord face failure (CFF). Welding parameters were optimised based on dilatometer results and thermal cycle limits ($t_{8.5} \leq 12$ s). Measurement techniques included strain gauges and digital image correlation (DIC) to quantify joint deformation by chord indentation. The force–indentation relationship was used to determine the ultimate strength of the joints. The results demonstrate the effects of steel grade, β-ratio, chord slenderness and preload on the load-bearing behaviour of the joints and provide a reliable basis for numerical modelling and future design recommendations for N-joints made of high-strength steel.

Keywords N-joints; high-strength steel; hollow section joints; punching shear failure; chord face failure; full-scale tests

1 Introduction

The increasing availability and use of high-strength steels in steel construction opens up considerable potential for increasing efficiency, in particular by saving resources and the associated reduction in CO_2 emissions. At the same time, the use of these materials poses new challenges in terms of design and fabrication – especially for welded hollow section joints. The existing design rules for welded hollow section joints in EN 1993-1-8 [1] are predominantly based on test data with steels of steel grade S355 and do not adequately capture the structural behaviour of high-strength steels. In the past, concerns have been raised about whether the generalised reduction in the load-bearing capacity of hollow section joints made from high-strength steel grades – according to prEN 1993-1-8 [2] – through the use of a lower material factor C_f (see Tab. 1), and the limitation of the nominal yield strength to the lesser of f_y or $0.8 \cdot fu$ for brittle failure mechanisms, may be overly conservative. These reductions limit the efficient use of high-strength steels and are based on a limited number of experimental and numerical investigations. They have not been sufficiently verified, especially for welded N-joints. In addition, the established 3% deformation criterion according to Lu et al. [3] for determining the load-bearing capacity of hollow section joints made of high-strength steels requires critical evaluation. In order to address this issue, a systematic experimental investigation of the structural behaviour of welded N-joints made of high-strength steels (S500MH, S700MH, S620QH, S770QH and S890QLH) was carried out in the FOSTA research project P1453 [4]. Within 13 full-scale tests on N-joints made of high-strength steel, the influence of various geometric parameters, steel grades, profile shapes and degree of pre-stressing of the chord was investigated to comprehensively record the real structural behaviour of N-joints until failure.

Particular attention was paid to the key failure mechanisms 'punching shear failure (PSF)' and 'chord face failure (CFF)'. The test results provide an essential basis for the validation of numerical models to carry out extended parametric studies and for further development of existing design formulae for the use of high-strength steels.

2 Test programme

The test programme on welded high-strength steel N-joints fabricated from hollow sections comprised 13 full-scale ultimate load tests. Hollow section joints made of five different steel grades were tested. The steel grades used are divided into hot-finished tempered hollow sections according to DIN EN 10210-3 [5] made of the steel grades S620QH, S770QH and S890QLH as well as cold-finished thermomechanically rolled and welded hollow sections according to DIN EN 10219-3 [6] made of the steel grades S500MH and S700MH. In addition, hollow section joints made of circular (CHS) and square (SHS) hollow sections were tested. In order to quantify

Tab. 1 Material factor for the design of welded hollow section joints according to prEN 1993-1-8 [2]

Scope of application	Material factor C_f
$f_y \leq 355$ N/mm²	$C_f = 1.00$
355 N/mm² $< f_y \leq 460$ N/mm²	$C_f = 0.90$
460 N/mm² $< f_y \leq 550$ N/mm²	$C_f = 0.86$
550 N/mm² $< f_y \leq 700$ N/mm²	$C_f = 0.80$

the influence of the chord utilisation in tension on the load-bearing capacity of the hollow section joints, three load-bearing capacity tests were carried out for the two different profile shapes (CHS, SHS) on a joint geometry with different degrees of chord preloading.

In the test programme, all specimens made of CHS have the same chord dimensions, only the brace dimensions vary and accordingly the β-ratio. For the specimens made of SHS, both the chord and brace dimensions vary and with them the β-ratio and the chord slenderness 2γ. An angle of $\theta_2 = 50°$ was selected for the diagonal tensional brace for all specimens. The N-joint geometry results in $\theta_1 = 90°$. In order to be able to produce a high-quality weld in the gap area, the gap size was specified to $g = 3 \cdot t_i$. The dimensions of the specimens were selected to eliminate the possibility of brace failure and weld failure. Therefore, the filler material G89, i.e., an overmatching ratio resp. an even-matching ratio for the steel grade S890QH, has been selected. Considering the weld type, for all specimens a full penetration butt weld was realised. In summary, the test programme for the full-scale ultimate load tests on welded high-strength N-joints is shown in Tab. 2. This includes the associated nominal geometric dimensions and dimensionless parameters.

3 Manufacturing of the specimens

3.1 Welding fabrication

Based on the results of the dilatometer tests on the steel grades used [4], a limit of the $t_{8,5}$ time of 12 s was selected for welding the specimens. This ensured that the softening observed in the dilatometer tests, particularly for steel grade S700MH, could be kept within limits and a suitable weld design could be assumed. Using the limit value of 12 s for the $t_{8,5}$ time, the maximum heat input was calculated in accordance with DIN EN 1011-2 [7] Appendix D and a preliminary welding procedure specification (pWPS) was prepared. To calculate the preheating temperature, the Carbon Equivalent Thyssen (CET) was determined according to DIN EN 1011-2 [7] C.3.2.1 from the chemical composition data of the factory certificates 3.1 according to DIN EN 10204 [8].

The pWPS was used to carry welding tests on T-joints made from the hollow sections used in the project. During the welding process, the actual $t_{8,5}$ times were measured with type K thermocouples, which were inserted into the weld bath or attached in the area of the heat-affected zone (HAZ) (Fig. 1). The results of the measurements in Tab. 3 show that the limit of the $t_{8,5}$ time was met or slightly exceeded in the case of the top layer using the welding parameters selected in the pWPS and the preheating temperature calculated via the CET. By further limiting the temperature of the intermediate layer, the specified $t_{8,5}$ times could also be achieved in the top layer.

In order to verify the pWPS, macrosections of the welds were made and hardness measurements according to DIN EN ISO 6507-1 [9] were carried out. For this purpose, sample areas have been selected in which the melt temperature was measured during the welding process

Tab. 2 Test programme of the full-scale ultimate load tests on welded high-strength N-joints

	Steel grade	Chord	Brace	2γ	β	g'	$\frac{e}{d_0}$	τ	n_0
CHS	S620QH	139.7 × 8.0	76.1 × 6.3	17.5	0.55	2.36	0.41	0.79	0.0
		139.7 × 8.0	88.9 × 6.3	17.5	0.63	2.36	0.54	0.79	0.0
	S770QLH	139.7 × 8.0	76.1 × 6.3	17.5	0.55	2.36	0.41	0.79	0.0
		139.7 × 8.0	76.1 × 6.3	17.5	0.55	2.36	0.41	0.79	0.5
		139.7 × 8.0	76.1 × 6.3	17.5	0.55	2.36	0.41	0.79	0.7
		139.7 × 8.0	101.6 × 6.3	17.5	0.72	2.36	0.66	0.79	0.0
	S890QLH	139.7 × 8.0	76.1 × 6.3	17.5	0.55	2.36	0.41	0.79	0.0
SHS	S500MH	120.0 × 7.0	90.0 × 6.0	17.1	0.75	3.00	0.71	0.86	0.0
	S700MH	100.0 × 5.0	70.0 × 3.0	20.0	0.7	1.80	0.64	0.60	0.0
		100.0 × 5.0	70.0 × 3.0	20.0	0.7	1.80	0.64	0.60	0.5
		100.0 × 5.0	70.0 × 3.0	20.0	0.7	1.80	0.64	0.60	0.7
		100.0 × 5.0	50.0 × 3.0	20.0	0.5	1.80	0.48	0.60	0.0
	S890QLH	100.0 × 5.6	70.0 × 5.6	17.9	0.7	2.84	0.66	1.00	0.0

Fig. 1 Measurement of the $t_{8,5}$ time with type K thermocouples [4]

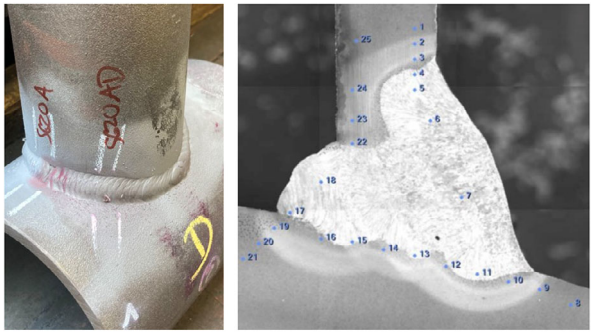

a) b)

Fig. 2 a) Position of a macrosection in specimen S620QH and b) macrosection of S620AD with position and numbering of the hardness indentations [4]

using thermocouples (see Fig. 2a, position S620AD). The macrosections produced (see Fig. 2b) show the proper execution of a butt weld with full penetration, but it is also evident, that the welding process results in an additional fillet weld.

The results of the hardness measurements HV10 according to DIN EN ISO 6507-1 [9] are shown in Fig. 3. Fig. 3a shows the results of the hardness measurements on the root layer, in which a $t_{8,5}$ time of max. 7.9 s was measured. Fig. 3b shows the results of the hardness measurements on the top layer, in which a $t_{8,5}$ time of max. 17 s was measured. On the one hand, the measurement results show an increased hardness in the weld metal (WM), which is due to the overmatching with the selected high-strength filler material G89. On the other hand, a decrease in hardness in the HAZ due to the welding process, which is typical for fine-grained structural steels, can be observed. Fig. 3 also shows that the drop-in hardness values in the HAZ of the brace are significantly higher than in the chord due to the smaller wall thickness (see measurement points 22–24, HAZ brace and measurement point 19, HAZ chord). An influence of different $t_{8,5}$ times of root and top layer of $\Delta = 9.1$ s is not determinable and thus confirms the results of the dilatometer tests for the quenched and tempered steel grade S620QH.

3.2 Geometry of the test specimens

The dimensions of the specimens were chosen on the basis of previous tests on hollow section joints [10]. The distance between the joint area and the supports of the test rig was chosen to be at least $l_{(i,0)} = 5 \cdot d_0$ or $l_i = 5 \cdot d_i$. If these dimensions are maintained, according to [10] the external influences of the test rig on the load-bearing capacity of the joint can be neglected and the flow of forces of a real truss joint is achieved in the area to be tested. As already described, the weld has been designed as a butt weld. On the one hand, this means that the failure mechanism of weld failure can be excluded, and on the other hand, preliminary numerical investigations have shown that the respective a-dimension of a fillet weld has a significant influence on the load-bearing capacity of the joint. The tests should therefore be carried out using a butt weld to represent the most unfavourable case with regard to the joint load-bearing capacity. Only the heel of the diagonal brace could not be butt-welded and therefore an a-dimension of $a = 1.5 \cdot t$ was specified. The weld preparation for the butt weld, the cutting of the hollow sections and the welding of the specimens was carried out by qualified service providers and steel fabricators within the research project P1453 [4] (see Fig. 4). The 3D intersection curve required for the weld preparation of the CHS profiles was produced using Computerized Numerical Control (CNC) plasma robots based on research project P1163 [11] (Fig. 5).

4 Execution of the tests

4.1 Test setup

Fig. 6 shows the test setup designed for the project as a 3D CAD model. In order to test the load-bearing capacity

Tab. 3 Welding parameters and measured or calculated values of the $t_{8,5}$ times of the welding tests on steel grade S620QH

Layer	Welding parameters					$t_{8,5}$ time	
	U	I	V	E	T_0	Measured	DIN EN 1011-2 [7]
	[V]	[A]	[mm/s]	[kJ/mm]	[°C]	[s]	[s]
Root layer	18.1–18.7	119–130	2.8–3.0	0.77–0.81	110	6.9–7.9	5.7–6.4
Top layer	18.8	116-117	1.7–1.8	1.21–1.26	130–140	15.8–17.0	16.7–17.0

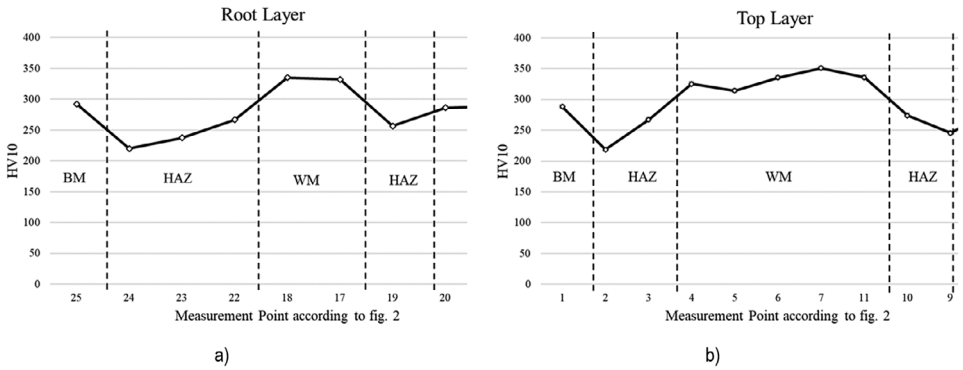

Fig. 3 Results of the hardness measurements HV10 on sample S620QH made of CHS for a) root layer and b) top layer

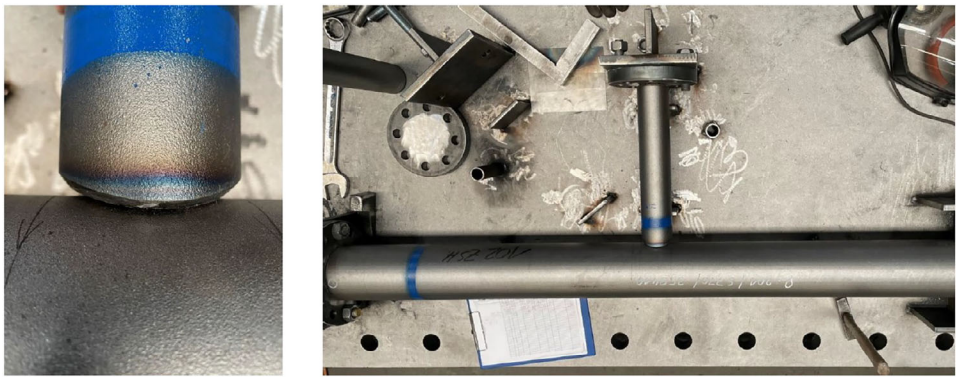

Fig. 4 Tacking of the specimens (CHS) [4]

of the N-joints, the force is applied to the vertical brace with a 2.5 MN cylinder (1) in a displacement-controlled manner. The support conditions selected for the test setup lead to a tensile reaction force in the diagonal brace that corresponds to the respective force in a real truss girder.

The bearing conditions of the N-joints are different for the two cases with preloading and without preloading of the chord (see Fig. 7). A vertical bearing (6) (see Fig. 8) was realised at the end of the specimen to prevent global rotation of the specimen due to the circumferential bearing of the specimen ends. This bearing was free to move in the longitudinal chord direction for the tests with chord preloading. For the tests without chord preloading, the chord was held longitudinally. In the static system, it is assumed that the tensional rods are acting like expansion springs.

The tension preloading of the chord was applied via four 1 MN pistons (2) attached horizontally to a tensioning jack via M90 tension rods (3), which were connected to the chord end by an eye-rod bolt connection. All resulting or applied loads were transferred and short-circuited into a pre-stressed concrete

Fig. 5 Cutting (3D intersection curve + weld preparation) of the CHS with CNC-controlled plasma cutting robots [4]

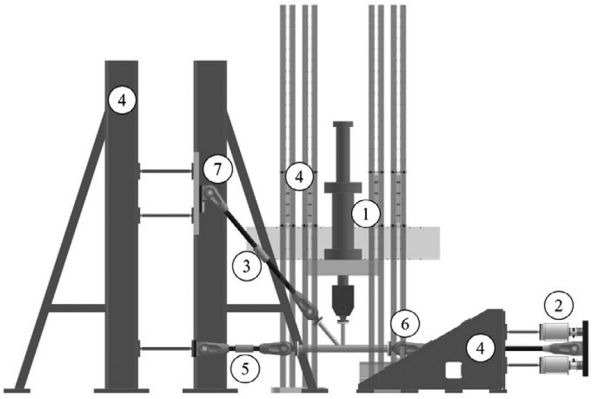

Fig. 6 CAD model of the test setup for testing the load-bearing capacity of N-joints [4]

ceiling via tension walls, the portal and tensioning jacks (4).

In order to avoid constraining forces in the braces, the length of the tension rods could be adjusted using turnbuckles (5). Before the actual test, a preload test was always conducted in order to measure the change in length depending on the respective preload applied to the chord using inductive displacement transducers. The chord was then relieved and the test specimen was displaced by the previously measured value in the opposite direction to the direction of tensile preloading. This also eliminated the influence of the elastic elongation of the tie rods and the stiffness of the bearings. After the chord was pre-tensioned, the vertical brace of the N-joint could be connected to the test cylinder without any constraint. The diagonal brace was connected in the same way with a length-adjustable tie rod. In addition, the support of the tie rod (7) (see Fig. 9a) could be adjusted in height to compensate for any manufacturing imperfections in the brace angle or gap dimension. At the same time, it was ensured for the different β-ratios of the specimens that there were no eccentric load flows and thus no secondary bending moments in the diagonal brace. Fig. 9b shows a CHS specimen installed in the test rig.

4.2 Measurement concept

In principle, force, displacement and strain were measured at different points during the test. The measurement concept for the N-joints is shown in Fig. 10. To determine the joint load-bearing capacity, the force applied to the vertical brace was measured using a load cell. In addition to the force, the displacement of the test cylinder was also measured, as well as the force and displacement of the pistons used to apply the pre-tension to the chord. Strain gauges were attached to the specimens to determine the strain distribution as a function of the applied force. The measurement concept for the investigated N-joints required the application of 16 strain gauges to each specimen. In order to measure the strains outside an area of potential influence of the different stiffnesses in the joint, the strain gauges were attached to the chord at a distance of $1\times\ D_0/D_i$ or $3\times\ D_0/D_i$ to the joint area. The measurement results of the strain gauges were used to validate the numerical models and thus the results of the calculations.

In order to evaluate the load-bearing capacity of the joint, it is a common practice to plot the force in the brace against the percentage of indentation of the brace into the chord. In this way, the local deformation of the joint is referred to and global deformations due to deformations of the test rig are eliminated. This emphasises the importance of measuring the indentation in this type of tests on hollow section joints. A digital image correlation (DIC) system supplied by *Limess* was used to measure the indentation. By defining two measuring points (MP1 and MP2, see Fig. 11b) on the brace and on the chord, the indentation of the brace into the chord can be measured. Displacements u_i of the two points occur due to the indentation of the brace into the chord member. These results from the global displacement of the chord and the local deformation of the chord top flange. By relating the difference between the two displacements to the initial length $l_{0,y}$, the global influence can be eliminated, resulting in the chord indentation (Eq. (1)).

$$\varepsilon_{\text{chord}} = \frac{u_{\text{MP2},y} - u_{\text{MP1},y}}{l_{0,y}} \cdot 100\% \tag{1}$$

where ε_{chord} is the chord indentation [%]; $u_{MP2,y}$ is the displacement in y-direction measuring point 2 [mm]; $u_{MP1,y}$ is the displacement in y-direction measuring point 1 [mm]; and $l_{0,y}$ is the initial length between the two measuring points [mm].

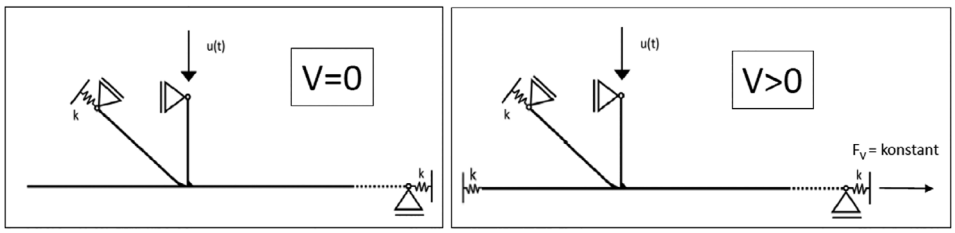

Fig. 7 Static systems of the N-joint with and without pre-tensioning of the chord [4]

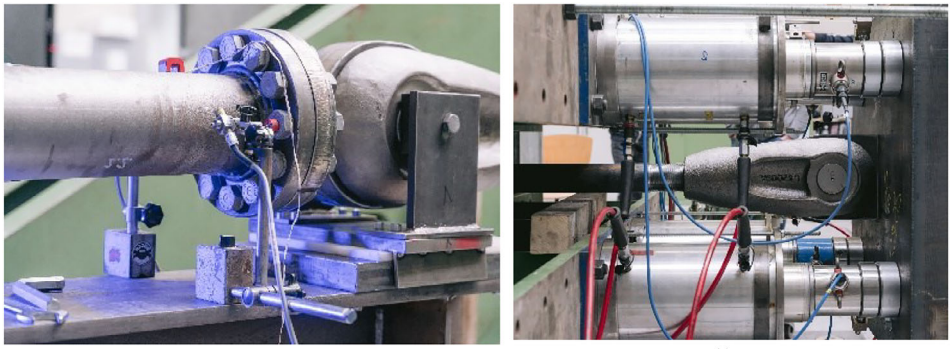

a) b)

Fig. 8 a) Vertical bearing (6) and b) application of the preload to the chord (2) [4]

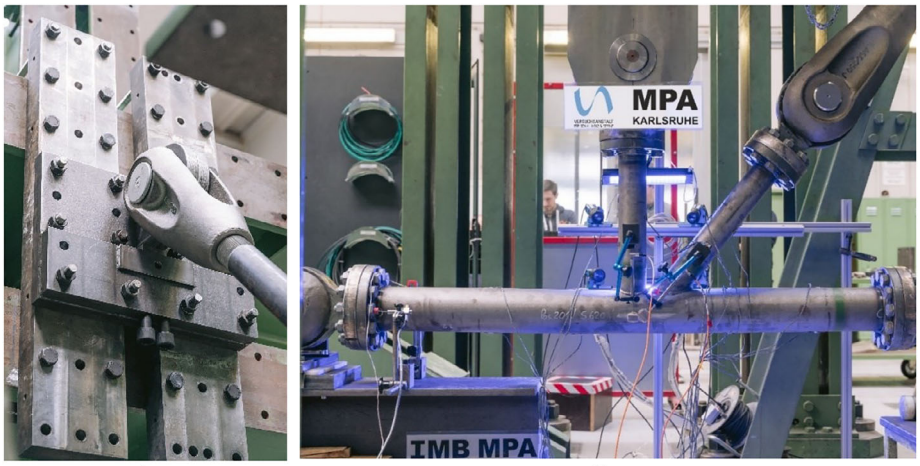

a) b)

Fig. 9 a) Height-adjustable bearing of the diagonal brace (7) and b) CHS specimen installed in the test rig [4]

To determine the joint load-bearing capacity, the force applied to the vertical brace was measured using a load cell. In addition to the force, the displacement of the test cylinder was also measured, as well as the force and displacement of the pistons used to apply the pre-tension load to the chord. Strain gauges were attached to the specimens to determine the strain distribution as a function of the applied force. The measurement concept for the investigated N-joints required the application of 16 strain gauges to each specimen. In order to measure the strains outside an area of potential influence of the different stiffnesses in the joint, the strain gauges were attached to the chord at a distance of $1\times\ D_0/D_i$ or $3\times\ D_0/D_i$ to the joint area. The measurement results of the strain gauges were used to validate the numerical models and thus the results of the calculations.

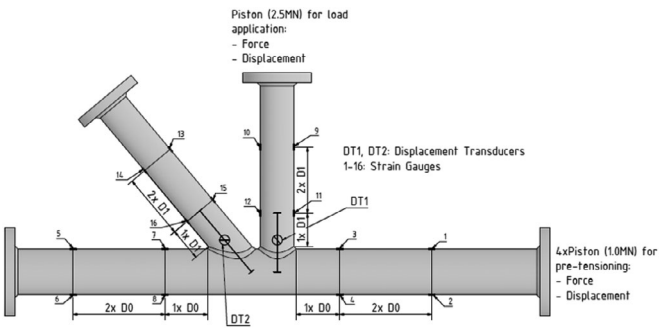

Fig. 10 Measurement concept

4.3 Evaluation of the test results

The joint load-bearing capacity is determined at the maximum of the force–indentation curve and thus at the point of the ultimate load. A criterion based on deformation, such as the 3% deformation criterion frequently used in the literature, is not used for the evaluation of the joint load-bearing capacity of N-joints made of high-strength steel. The 3% deformation criterion according to Lu et al. [3] was initially developed for the evaluation of T-joints made of structural steels with normal strength grades. T-joints or X-joints with small β-ratios whose braces are subjected to axial compression do not show a maximum or ultimate load in the load–indentation curve. The reason for this is the activation of membrane stresses in combination with resulting large plastic strains. If the T-joints fail in these cases, the joint area of the specimens is deformed to such a large extent that the serviceability of the joint is already questionable. For this reason,

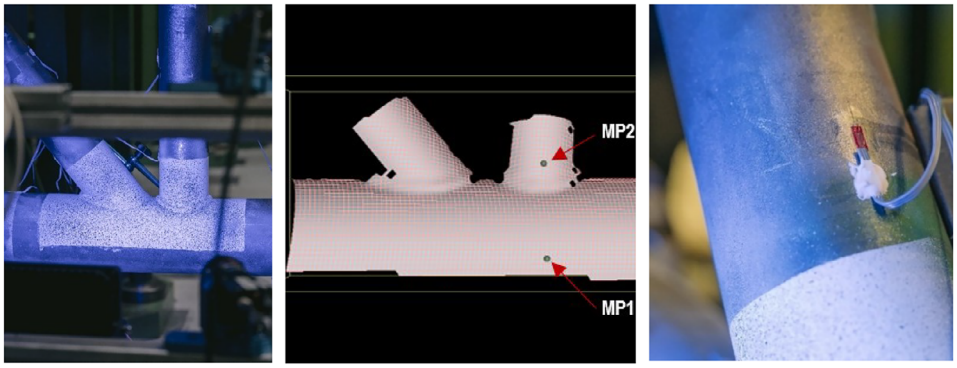

Fig. 11 a) Stochastic pattern, b) mesh in the ISTRA 4D software with the two selected measuring points, and c) strain gauge application [4]

the joint load-bearing capacity for these type of joints is determined using the 3% deformation criterion of Lu et al. [3]. The test results on N-joints made of high-strength steels show, on the one hand, that an ultimate load due to an abrupt failure caused by the tensional brace tearing out of the chord (PSF) is always observed. On the other hand, an indentation of 3% is sometimes not achieved at all. For this reason, the load-bearing capacity of the joint is determined on the basis of the ultimate load at failure.

5 Test results

Fig. 12a shows the test results of the high-strength N-joints made of CHS and SHS without pre-tensioning of the chord. Only the force–indentation curve of the vertical compressive brace is shown. The force–indentation curves show the following findings: firstly, the curves differ between the CHS and SHS specimens. The SHS specimens exhibit significantly larger deformations until specimen failure. The 2γ-ratio and the dimension of the gap are constant for the CHS specimens, meaning that the initial stiffness depends only on the β-ratio. The results of the tests on the specimens with the numbers 1, 3 and 7 inhibit the same initial stiffness due to the constant β-ratio (the three specimens differ only in the steel grade). When the β-ratio is increased, as in the case of specimens 2 and 6, the initial stiffness also increases. The results for the specimens numbered 1, 3 and 7 show an increasing load-bearing capacity of the joint with an increasing yield strength of the material used.

The results of the tests with pre-tensioning also show the expected decrease in joint load-bearing capacity as the degree of utilisation due to pre-tensioning increases (see Fig. 12b), regardless of the profile shape (CHS or SHS). prEN 1993-1-8 [2] distinguishes between several failure mechanisms. Due to the choice of profile and the dimensions of the specimens, some failure mechanisms were excluded during the test design phase. Consequently, according to prEN 1993-1-8 [2], only two failure mechanisms, PSF and CFF, could occur. According to prEN 1993-1-8 [2], the joint load-bearing capacity is calculated for both failure mechanisms, whereby the smaller value of the joint load-bearing capacity is decisive for the verification of the structural resistance of the joint. The decisive failure mechanisms according to

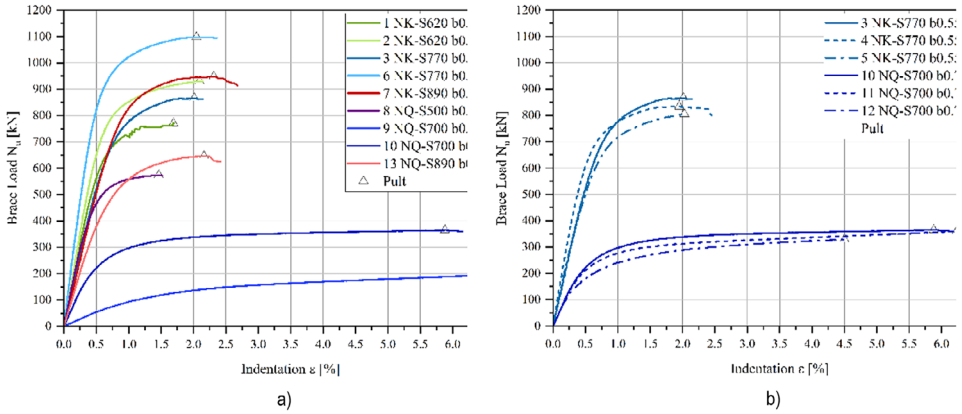

Fig. 12 Test results of the high-strength N-joints made of CHS and SHS a) without pre-tensioning of the chord and b) with pre-tensioning of the chord [4]

Tab. 4 Comparison of the test results with the design rules according to prEN 1993-1-8 [2]

Shape	Nos.	Labelling	$N_{Rd,prEN}$ [kN]	FM[a] standard	P_{ult} [kN]	FM[a)] test	$P_{ult}/N_{Rd,prEN}$
CHS	1	1 NK-S620 b0.55 V0	596.26	CFF	770.56	CFF + PSF	1.29
	2	2 NK-S620 b0.63 V0	709.79	CFF	930.35	CFF + PSF	1.31
	3	3 NK-S770 b0.55 V0	690.93	PSF	866.38	CFF + PSF	1.25
	4	4 NK-S770 b0.55 V0.5	677.19	PSF	834.15	CFF + PSF	1.23
	5	5 NK-S770 b0.55 V0.7	648.47	CFF	805.73	CFF + PSF	1.24
	6	6 NK-S770 b0.72 V0	873.44	PSF	1098.12	CFF + PSF	1.26
	7	7 NK-S890 b0.55 V0	775.95	PSF	948.37	CFF + PSF	1.22
SHS	8	8 NQ-S500 b0.75 V0	401.14	CFF	573.8	CFF + PSF	1.43
	9	9 NQ S700 b0.5 V0	190.78	CFF	238.25	CFF + PSF	1.25
	10	10 NQ S700 b0.7 V0	265.84	CFF	364.90	CFF + PSF	1.37
	11	11 NQ S700 b0.7 V0.5	253.39	CFF	359.12	CFF + PSF	1.42
	12	12 NQ S700 b0.7 V0.7	233.73	CFF	328.49	CFF + PSF	1.41
	13	13 NQ S890 b0.7 V0	559.79	CFF	646.54	CFF + PSF	1.15

[a)] Failure mechanism

prEN 1993-1-8 [2] and the associated joint load-bearing capacities, determined with the real material properties and measured geometric dimensions, are given in Tab. 4. The geometric dimensions of the specimens were determined by optical measurement with a hand-held laser and the material properties were determined by means of tensile tests. Tab. 4 also shows the load-bearing capacity of the specimens as well as a comparison of the design resistances calculated according to prEN 1993-1-8 [2] with the experimentally determined characteristic joint load-bearing capacities. The experimentally determined joint load-bearing capacities are always higher than the resistances calculated according to [2]. Results exceed the design values in a range between 15 and 43%.

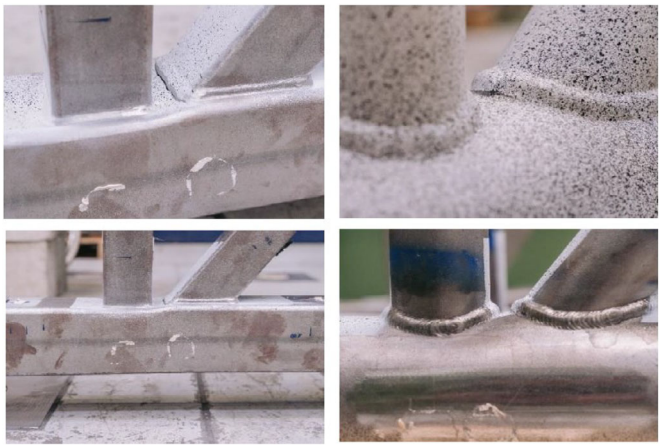

Fig. 13 Failure mechanisms of the tested N-joints [4]

Contrary to the clear distinction between the failure mechanisms in prEN 1993-1-8 [2], the tests showed that a combined failure due to CFF and PSF always occurred (Fig. 13). Initially, there was an indentation of the vertical brace into the chord (plastification of the chord). As the load increased, a crack initiated at the tip of the crown of the tensional diagonals, which led to a tear through the chord wall and thus to joint failure finally.

The tests were stopped at the first drop of load, as a preliminary test showed that the resulting crack rapidly continues to grow through the chord due to the pretensioning of the chord, resulting in a tensile/shear failure of the entire chord (Fig. 14). This preliminary test has shown that this is a particularly critical failure. If the test results are thus transferred to a truss structure, a global failure of the entire supporting structure occurs [12].

The DIC measurements showed that an initial crack initiated at the top of the chord at a quite early stage during the test. This crack continues to grow during the test until the crack tears through the chord wall (Fig. 15). After formation of this initial crack, the load increases only slightly. However, large deformations occur up to fracture and a drop of load occurs associated with specimen fracture. The preliminary numerical investigations have shown that the highest stress multiaxialities as well as largest plastic strains occur at the respective point where the initial crack occurs in the test. Mechanic material tests have shown that the critical plastic strain decreases with increasing stress multiaxiality until damage initiation or failure [12]. This relationship is used in the numerical models to determine the time of crack initiation or PSF using a break-off criterion [13].

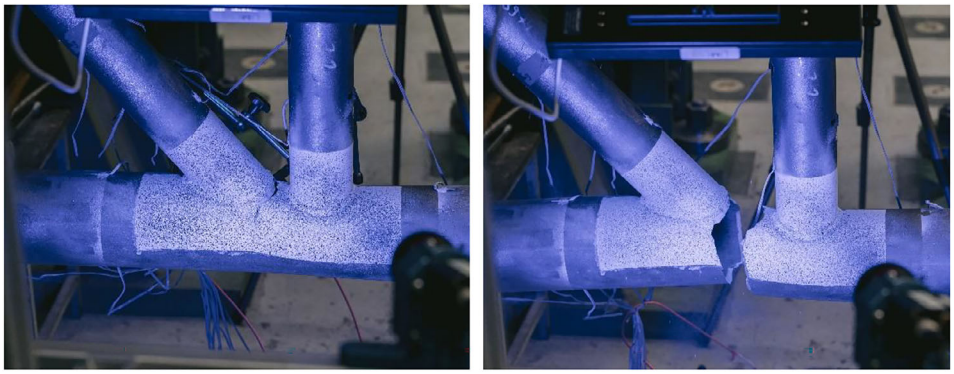

a) b)

Fig. 14 a) Crack growth in the chord profile and b) failure of the chord [4]

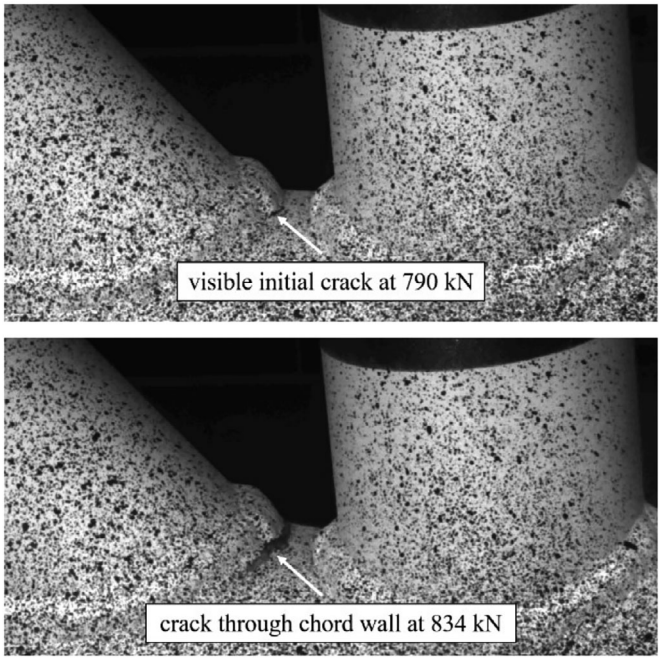

Fig. 15 Crack initiation and tearing through the chord wall observed during the test with the DIC

5.1 Statistical evaluation of the test results according to DIN EN 1990

Due to the scattering of the input variables (geometry dimensions and material properties), the test results were statistically analysed in accordance with DIN EN 1990 [14] Appendix D. The coefficients of variation of the scattering variables were taken from [15]. According to [15], a value of $\gamma_m = 1.1$ is assumed due to the uncertainty of measurement. The statistical evaluation is carried out separately for the two failure mechanisms of CFF plastification and PSF, depending on which failure mechanism is decisive according to prEN 1993-1-8 [2] (see Tab. 4). The influence of joint eccentricity was neglected when determining the joint load-bearing capacity according to prEN 1993-1-8 [2].

The results of the statistical analysis are shown in Fig. 16a for CHS and in Fig. 16b for SHS. Fig. 16 shows a minimum statistical coefficient ζ_c/γ_M of 0.95 for the tests on the N-joints made of SHS. This statistical coefficient can be compared with the C_f-factor specified in prEN 1993-1-8 [2] and thus the necessity of the material factor can be assessed. The test results show that even the

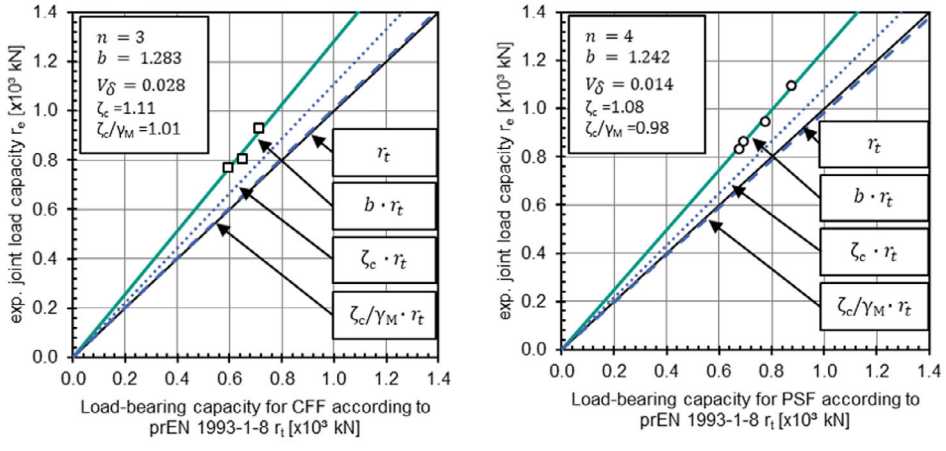

a) b)

Fig. 16 Statistical evaluation according to DIN EN 1990 [14] of the test results for CHS: a) chord face failure b) punching shear failure [4]

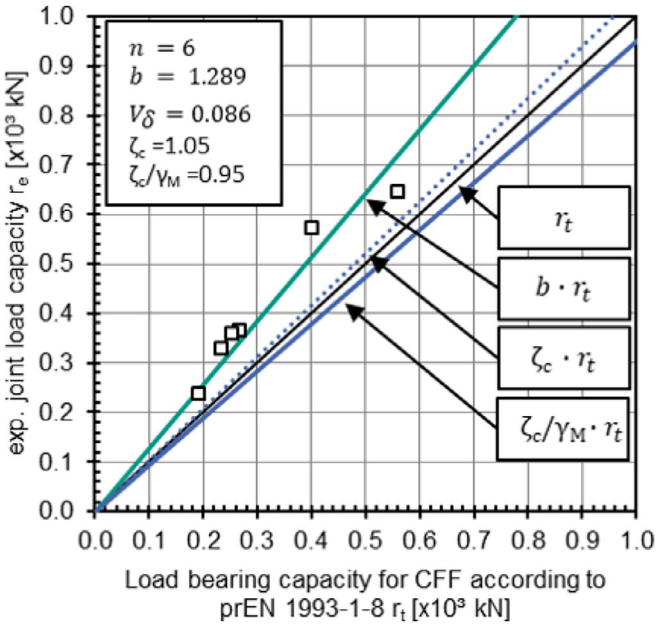

Fig. 17 Statistical evaluation according to DIN EN 1990 [14] of the test results for SHS [4]

minimum resulting statistical coefficient $\zeta_c/\gamma_M = 0.95$ for the test results on N-joints made of SHS (Fig. 17) is significantly higher than the value of the C_f-factor of $C_f = 0.8$ for steels with a yield strength above 550 MPa.

This result shows the tendency that the C_f-factor can be adjusted. However, the number of tests carried out and the variation of the influencing parameters are too small to be able to make a reliable statement only based on the test results. For further evaluation of the existing design equations according to prEN 1993-1-8 [2] and for the influence of the dimensionless parameters, supplementary numerical parametric studies have therefore been carried out [4, 16].

6 Summary and conclusion

This article presents a comprehensive experimental investigation of welded N-joints made of high-strength hollow sections using five different steel grades and two different profile shapes (CHS and SHS). Thirteen large-scale tests were carried out to examine the influence of key parameters such as steel grade, β-ratio, chord slenderness, and pre-tensioning on joint performance. The test setup and measurement approach – including digital image correlation and strain gauge instrumentation – enabled a detailed analysis of deformation and failure mechanisms of welded N-joints made of high-strength steels. The results reveal that current design provisions in prEN 1993-1-8 [2] underestimate the load-bearing capacity of high-strength N-joints, as the experimentally determined ultimate loads exceeded the design values by 15–43%. A combined failure mode of CFF and PSF was consistently observed, contradicting the discrete classification of failure modes assumed in the design standard. The statistical evaluation of the test results further supports the potential for adjusting the material factor (C_f) currently prescribed for high-strength steels.

In conclusion, the findings provide valuable insights into the structural and failure behaviour of N-joints made of high-strength steel and demonstrate the need for revised design provisions. The experimental results offer a solid foundation for the validation of numerical models and the development of enhanced design guidelines that facilitate the efficient and reliable use of high-strength steel in hollow section joints.

Acknowledgements

The research project 'Design and execution of hollow section joints made of high-strength steels using the example of N-joints' was funded by the Federal Ministry of Economic Affairs and Climate Action as part of the 'Industrial Collective Research' programme based on a resolution of the German Bundestag. This project 01IF21498N/P1453 from the Research Association for steel Application (FOSTA), Düsseldorf, was carried out at Karlsruhe Institute of Technology, KIT Steel and Lightweight Structures. The authors are grateful to the Research Association for Steel Application (FOSTA) for their financial support as well as all the industry partners for supplying materials and performing the welding work.

Open access funding enabled and organized by Projekt DEAL.

References

[1] DIN EN 1993-1-8:2010-12 (2010) *Eurocode 3: Bemessung und Konstruktion von Stahlbauten - Teil 1-8: Bemessung von Anschlüssen; Deutsche Fassung EN 1993-1-8:2005 + AC:2009*. Berlin: Beuth Verlag GmbH.

[2] prEN 1993-1-8:2021-03 (2021) *Eurocode 3: Bemessung und Konstruktion von Stahlbauten - Teil 1-8: Bemessung von Anschlüssen; Deutsche und Englische Fassung prEN 1993-1-8:2021*. Berlin: Beuth Verlag GmbH.

[3] Lu, L. H.; Winkel, G. D.; Yu, Y.; Wardenier, J. (1994) *Deformation limit for the ultimate strength of hollow section joints*. Grundy, P.; Holgate, A.; Wong, B. [eds.] *Tubular Structures VI: Proceedings of the 6th International Symposium on Tubular Structures*. Melbourne, Australia: Routledge.

[4] Ummenhofer, T. et al. (2024) *Design and execution of hollow section joints made of high-strength steels using the example of N-joints, FOSTA research project P1453*.

Düsseldorf: Forschungsvereinigung Stahlanwendung e.V. (FOSTA).
[5] DIN EN 10210-3:2020-11 (2020) *Warmgefertigte Hohlprofile für den Stahlbau - Teil 3: Technische Lieferbedingungen für höher- und wetterfeste Stähle; Deutsche Fassung EN 10210-3:2020*. Berlin: Beuth Verlag GmbH.
[6] DIN EN 10219-3:2020-11 (2020) *Kaltgeformte geschweißte Hohlprofile für den Stahlbau - Teil 3: Technische Lieferbedingungen für höher- und wetterfeste Stähle; Deutsche Fassung EN 10219-3:2020*. Berlin: Beuth Verlag GmbH.
[7] DIN EN 1011-2:2001-05 (2001) *Empfehlungen zum Schweißen metallischer Werkstoffe - Teil 2: Lichtbogenschweißen von ferritschen Stählen*. Berlin: Beuth Verlag GmbH.
[8] DIN EN 10204:2005-01 (2005) *Metallische Erzeugnisse - Arten von Prüfbescheinigungen; Deutsche Fassung EN 10204:2004*. Berlin: Beuth Verlag GmbH.
[9] DIN EN ISO 6507-1:2018-07 (2018) *Metallische Werkstoffe - Härteprüfung nach Vockers - Teil 1: Prüfverfahren (ISO 6507-1:2018); Deutsche Fassung EN ISO 6507-1:2018*. Berlin: Beuth Verlag GmbH.
[10] Yao, Z.; Wilkinson, T. (2015) *Experimental investigation of the static capacity of grade C450 RHS K and N truss joints*. Batista; Vellasco; Lima; [eds.] *Tubular Structures XV, Proceedings of the 15th International Symposium on Tubular Structures, Rio de Janeiro, Brazil*.
[11] Kuhlmann, U. et al. (2020) *Wirtschaftliche Auslegung von ermüdungsbeanspruchten, geschweißten Rundhohlprofilknoten unter Berücksichtigung der erforderlichen Schweißnahtqualität* in: *Forschungsbericht FOSTA P1163 /IGF-Nr. 18883 BG*. Düsseldorf: Forschungsvereinigung Stahlanwendung e. V. (FOSTA).
[12] Engelhardt, I.; Ummenhofer, T.; Kuhlmann, U. (2024) *High-Truss (Hochfeste Hohlprofilfachwerke)* in: *Forschungsvorhaben HighTRUSS /FKZ Nr. 03TN0022*. Jülich: Projektträger Jülich, WIPANO.
[13] Schmidt, J. et al. (2025) *Numerical investigations of N-Joints from high-strength square hollow sections*. Steel Construction 18, No. 3, pp. 150–163. https://doi.org/10.1002/stco.202500023
[14] DIN EN 1990:2021-10 (2021) *Eurocode: Grundlagen der Tragwerksplanung; Deutsche Fassung EN 1990:2002_+ A1:2005_+ A1:2005/AC:2010*. Beuth Verlag GmbH.
[15] Fleischer, O. (2014) *Axial beanspruchte K-Knoten aus dünnwandigen Rechteckhohlprofilen* [Dissertation]. Karlsruher Institut für Technologie.
[16] Münch, A. (in prep.) *Bemessungskonzept zur Bestimmung der Tragfähigkeit hochfester Hohlprofilknoten* [Dissertation]. Karlsruher Institut für Technologie, Karlsruhe.

Authors

Adrian Münch, M.Sc. (corresponding author)
adrian.muench@kit.edu
Karlsruhe Institute of Technology
KIT Steel and Lightweight Structures
Otto-Ammann-Platz 1
76131 Karlsruhe
Germany

Dr.-Ing. Philipp Weidner
philipp.weidner@kit.edu
Karlsruhe Institute of Technology
KIT Steel and Lightweight Structures
Otto-Ammann-Platz 1
76131 Karlsruhe
Germany

Prof. Dr.-Ing. Thomas Ummenhofer
thomas.ummenhofer@kit.edu
Karlsruhe Institute of Technology
KIT Steel and Lightweight Structures
Otto-Ammann-Platz 1
76131 Karlsruhe
Germany

How to Cite this Paper

Münch, A.; Weidner, P.; Ummenhofer, T. (2025) *Experimental investigations of N-joints made of high-strength hollow sections*. Steel Construction 18, No. 3, pp. 139–149.
https://doi.org/10.1002/stco.202500021

This paper has been peer reviewed. Submitted: 11. June 2025; accepted: 10. July 2025.